

Quantitative geothermal interpretation of electrical resistivity models of the Rathlin Basin, Northern Ireland

R. Delhaye^{a,b,*}, V. Rath^a, A.G. Jones^{a,1}, M.R. Muller^{a,2}, D. Reay^c

^a Dublin Institute for Advanced Studies (DIAS), 5 Merrion Square, Dublin 2, Ireland

^b National University of Ireland, Galway, University Road, Galway, Ireland

^c Geological Survey of Northern Ireland (GSNI), Belfast, UK

ARTICLE INFO

Keywords:
Geophysics
Magnetotellurics
Geothermal exploration
Sedimentary basin
Ireland

ABSTRACT

In the evaluation of low- to medium-enthalpy geothermal resources on the island of Ireland, some of the most interesting targets are the deep sedimentary basins of Northern Ireland. The deepest of these is the Rathlin Basin, where Permian and Triassic reservoir sediments are known to exist to at least 2300 m depth. Two deep boreholes within the basin provide evidence of elevated temperatures at depth that are atypical within Ireland, prompting further geophysical exploration of the basin as one component of the IREtherm project. The magnetotelluric (MT) method was selected as the investigative geophysical tool as it is capable of sensing and defining electrically conductive porous sediments beneath overlying resistive strata, in this case flood basalts sequences. MT data were acquired on a rectangular grid of 39 sites across almost half of the onshore basin to investigate the composition and spatial variation of the basin's formations.

One-dimensional stochastic inverse modelling of the observed MT data was with a reversible-jump Markov chain Monte Carlo 1D inversion code, resulting in ensembles of models for each site. The use of model ensembles rather than single models avoids the pitfall of over-reliant interpretation on non-unique resistivity models, increasing the robustness of the interpretation. Interpreted models compare very favourably with nearby deep borehole records, and interpolation of the complete set of ensemble interpretations results in a conservative reservoir volume of approx. 32 km³ of combined Permian and Triassic sandstones beneath the MT survey.

Based upon new, high quality temperature data available in the Ballinlea 1 borehole, an approximate estimation of thermal energy in place as a function of final reservoir temperature has been performed for the interpreted MT resistivity model volume. A final minimum temperature of 25 °C (being the temperature that comparable estimates have been made for adjacent geothermal prospects) results in a minimum estimated Indicated Geothermal Reserve (IGR) of 2.9×10^{18} J beneath the MT survey area. The modelling results suggest that exploitation of the maximum volume of sediments would occur for a final temperature of ≈ 55 °C.

1. Introduction

The Rathlin Basin is a significant sedimentary depocentre in Northern Ireland (Fig. 1), comprising a succession of Carboniferous to Cretaceous strata. Permian and Triassic sandstone formations within the basin are known to act as hydrocarbon reservoir formations offshore, in the Irish Sea to the east (Richardson and Neymeyer, 2013). Equilibrated temperature measurements in two local boreholes – Port More 1 (PM1) and Ballinlea 1 (B1), respectively – in the basin show elevated geothermal gradients in comparison to the mean regional gradient, suggesting that the porous sediments function as a geothermal

aquifer. As hydrothermal fluid is typically saline and thus conducts electrons well, if the porous sediments are saturated with a hydrothermal brine and the fluid is sufficiently connected, they should be electrically distinct to the surrounding basal material and overlying aquitard formation and be resolved using appropriate deep-probing electromagnetic methods.

Several sets of geophysical data have previously been acquired across the basins of Northern Ireland, including gravity data, seismic reflection data, and most recently regional airborne geophysical data (aeromagnetic, radiometric and frequency-domain electromagnetic data). However, both the seismic reflection data and aeromagnetic data

* Corresponding author at: Dublin Institute for Advanced Studies (DIAS), 5 Merrion Square, Dublin 2, Ireland.

E-mail address: r.delhaye@cp.dias.ie (R. Delhaye).

¹ Now at: Complete MT Solutions Inc. (CMTS), Ottawa, Canada.

² Now at: Private Consultant, Cambridge, UK.

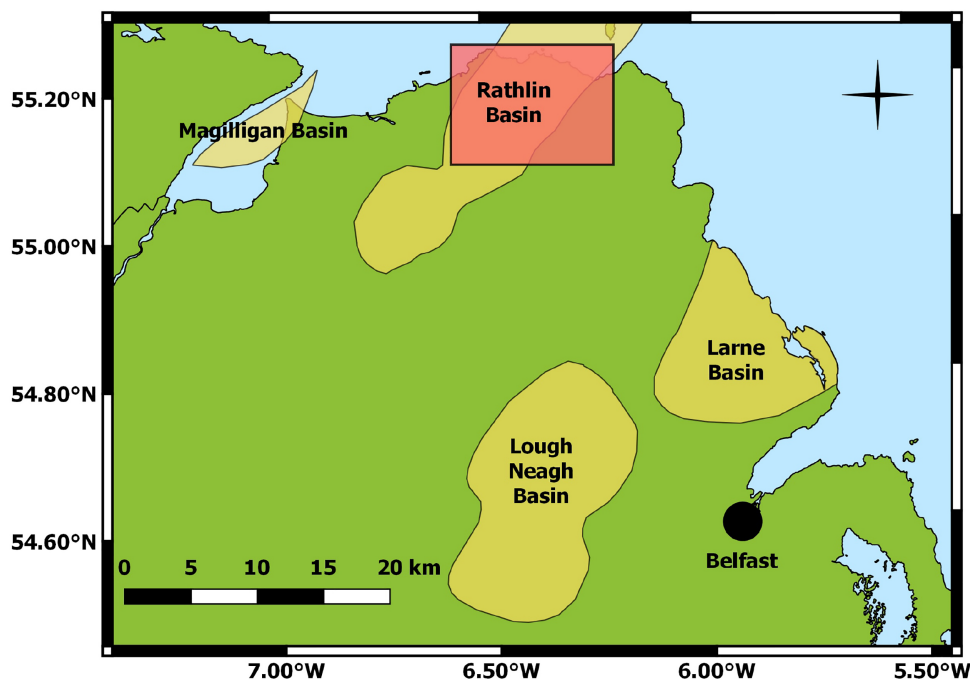


Fig. 1. Regional map of onshore sedimentary basins (yellow) within Northern Ireland (Belfast shown for location). The area of research considered in this article is shown by the red rectangle over the Rathlin Basin.

are dominated by the regionally present Antrim Lava group due to (1) its negative acoustic impedance contrast with respect to the underlying stratigraphy and irregular internal geometry at its base, and (2) its significant magnetic signature, respectively. Regional gravity data have been modelled, with results published in [Mitchell \(2004\)](#) that attribute a maximum depth of ~ 4 km to the base of the Permian and Triassic sediments; the authors of [Mitchell \(2004\)](#) note that this model assumes relatively low density Carboniferous sediments as observed in the adjacent Magilligan Basin to the west (see Fig. 1). If the Carboniferous sediments within the Rathlin Basin are of higher density than those of the Magilligan Basin then a greater thickness of the lower density Permian and Triassic formations would be required to remain consistent with the observed gravity anomaly.

Existing resistivity wireline logs from one of the boreholes confirm the electrical distinction of formations, suggesting that methods sensing lateral and vertical variation in electrical conductivity may be very productive. Hence, natural-source electromagnetic surveying using the magnetotelluric (MT) method of exploration of the onshore portion of the basin was carried out to evaluate the low- to medium-enthalpy geothermal potential of the Rathlin Basin.

In order to improve the accuracy of recovered resistivities from the modelling of MT data, the MT data were treated prior to inversion modelling for a form of galvanic electric field distortion known as “static-shift”. MT data are affected by near-surface resistivity structure below the resolution of the method, resulting in biased estimates of the electric field, and accordingly MT impedances “static-shift”-type distortion, as described in e.g. [Berdichevsky and Dmitriev \(1976\)](#); [Jones \(1988\)](#); [Chave and Jones \(2012\)](#). A number of approaches have been developed to compensate for this distortion, and as our survey area fortunately falls within the area covered by the regionally available airborne EM data from the Tellus Project ([Young, 2016](#)), we successfully adapted the method of [Pellerin and Hohmann \(1990\)](#). The method of [Pellerin and Hohmann \(1990\)](#) originally modelled ground-based time domain EM measurements to find a simple near-surface one-dimensional (1D) structure, and MT data were shifted to match the responses of this simple structure. We have adapted this approach by modelling airborne frequency domain EM (FDEM) data in place of the ground-based time domain EM data; specifically, we determine a best-fitting

single layer half-space resistivity model from the four frequency data at each measurement location, then collate these individual models into the top layers of a 3D resistivity forward model. The magnitudes of the MT responses from the forward model (i.e. the apparent resistivities) are compared with those of the observed data, and corrective factors δ_{Ex} , δ_{Ey} were found to reconcile the observed to calculated magnitudes. Full details of our approach to static-shift correction are presented in [Delhaye et al. \(2017\)](#).

This study presents the results of one-dimensional (1D) modelling of the MT data acquired over the northern half of the onshore part of the Rathlin Basin, and a geothermal interpretation of the basin in the context of existing geological and geophysical constraints. It follows the methodological study of static-shift correction of relevant MT data presented in [Delhaye et al. \(2017\)](#). Comparisons of models from the static-shift-corrected and original MT data show improved recovery of layer depths and thicknesses when compared to borehole information in this area, and hence all the results presented here were derived from the static-shift corrected MT data. In this paper we present an overview of the current knowledge of the basin, followed by an interpretation of 1D resistivity models derived from the MT data over the basin with respect to the existing knowledge. In conjunction with new temperature data acquired within the basin, the interpreted resistivity models are used to estimate the geothermal reservoir volume and associated geothermal heat energy in place.

2. Tectonic and geologic setting

The surficial geology of the Rathlin Basin is dominated by Paleogene volcanics that conceal much of Northern Ireland's older geological formations. A map showing the surficial geology of the survey area is presented in Fig. 2, together with borehole and MT site locations, modelling profiles, and the surface trace of the major Tow Valley Fault. The geology of the Rathlin Basin is described in detail in [Mitchell \(2004\)](#). The Rathlin Basin lies within one of the seven identifiable terranes that comprise modern-day Ireland; specifically, the basin lies within a region consisting of mid- to late-Neoproterozoic (1000–545 Ma) metamorphic and metasedimentary rocks collectively termed the Dalradian Supergroup. Due to extensive deformation and

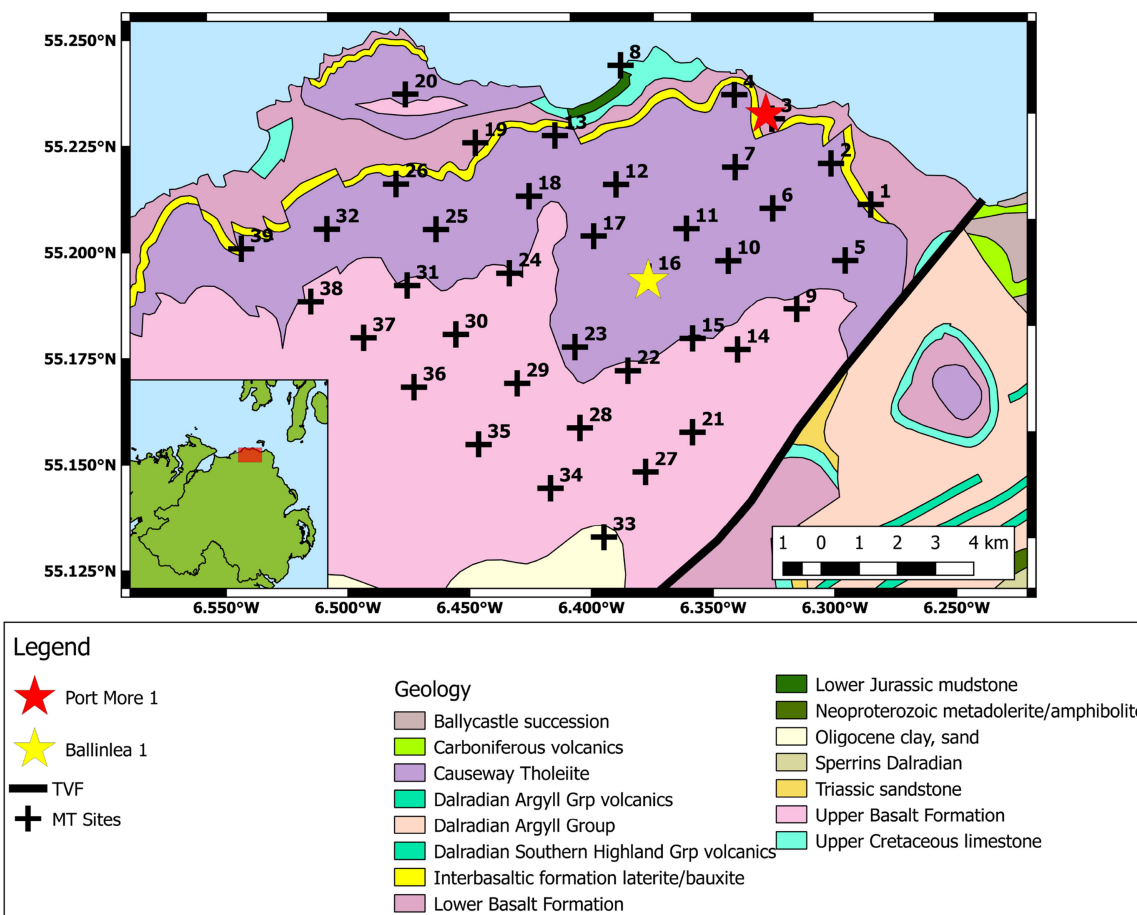


Fig. 2. Surficial geology of the Rathlin Basin survey area in Northern Ireland, overlain by magnetotelluric (MT) acquisition sites (numbered black pluses) and borehole locations (PM1, red star on the north-east coast, B1, yellow star further inland). The bold black line shows the location of the Tow Valley Fault. (For interpretation of the references to colour in this figure legend, the reader is referred to the web version of the article.)

metamorphism associated with the Grampian orogeny (475–470 Ma), the Dalradian rocks are expected to have reduced levels of hydraulic porosity and permeability, and hence elevated electrical resistivities. During the subsequent Variscan orogenic cycle (350–250 Ma), regional shear and stress reactivated the pre-existing Caledonian (490–390 Ma) Tow Valley Fault (TVF). The resulting normal and dextral strike-slip faulting created the rift basin that would later fill with Carboniferous, Permian and Triassic aged sediments to become the Rathlin Basin.

3. Stratigraphy

Stratigraphic information relevant to our study is mainly derived from the two deep boreholes within the basin, Port More 1 and Ballinlea 1 (locations in Fig. 2; see Fig. 3 for Port More 1 borehole stratigraphy). As the base of the Rathlin Basin sedimentary fill has not yet been reached by drilling, Carboniferous sediments encountered in the Ballinlea 1 borehole are assumed to be the basal lithology sediments. The assumption of basal sediments is supported by the presence of Carboniferous formations in the adjacent, shallower Magilligan Basin (locality in Fig. 1). Above the Carboniferous strata lie two Permian formations, the early-Permian Enler (EG) and Belfast (BG) groups, of interest as the formations have been observed to have favourable hydraulic properties for hydrocarbon reservoirs (Naylor and Shannon, 2011). The BG is overlain by the early-Triassic Sherwood Sandstone Group (SSG), with hydraulic properties comparable to the underlying BG. The SSG is overlain by the late-Triassic Mercia Mudstone group (MMG), which in turn is overlain by the early-Jurassic Lower Lias group (LLG) mudstones. However, the PM1 borehole encountered a

significant thickness of dolerite and basalt sills between the LLG and MMG formations, and the spatial extent of these intrusions is unknown across the basin. The youngest sediments within the basin are early-Cretaceous Ulster White Limestone formation (UWLF) cherts, overlying the LLG. Finally, the entire basin is concealed beneath the Antrim Lava group (ALG) of Paleogene flood basalts, which forms part of the North Atlantic Igneous Province (Mitchell, 2004). The age ranges of these formations are shown in Table 1.

4. Boreholes

To date two near-vertical boreholes have been drilled to significant depth within the onshore Rathlin Basin, namely, the aforementioned Port More 1 (PM1, 1967) and Ballinlea 1 (B1, 2008) boreholes (locations in Fig. 2), with measured total depths of ≈ 1900 and ≈ 2700 m below surface respectively. Wireline log data, detailed lithological logs and temperature measurements to 1481 m depth are publically available from the PM1 borehole. Equilibrated (i.e. at sufficient post-drilling time such that borehole fluids are in thermal equilibrium with adjacent rock - an equilibration period of 10–20 times the drilling time has been suggested by Bullard (1947), Beardmore and Cull (2001)) temperature measurements from the B1 borehole have also been recently acquired by Schlumberger on behalf of Rathlin Energy (UK) Ltd.

4.1. Port More 1 borehole

The PM1 borehole was drilled in 1967 to a near-vertical depth of 1900 m below surface to explore for coal and evaporite minerals at

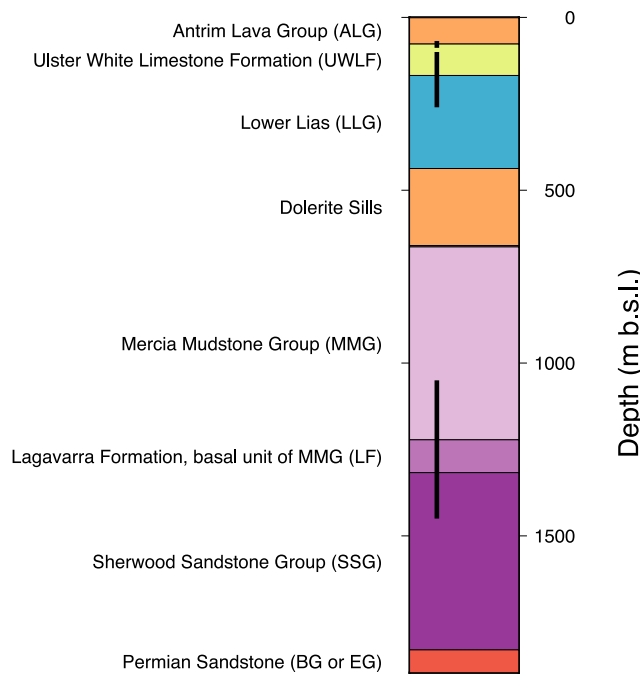


Fig. 3. Formations encountered in the PM1 borehole (see Fig. 2 for location). The borehole terminated at 1900 m depth, within Permian sandstones. It is unclear whether the Permian sandstones are of the Belfast (hydraulically favourable) or Enler group (less hydraulically favourable). Due to technical difficulties regarding the diameter of the hole, wireline logs were only acquired in several depth ranges; these intervals are marked by the solid black vertical lines.

Table 1

Ages and petrographic descriptions of the formations in the Rathlin Basin. Age is listed by both epoch and millions of years. Values and descriptions taken from Mitchell (2004).

| Formation | Epoch | Age (Ma) | Petrography |
|---|----------------|----------|-------------------------------------|
| Antrim Lava group (ALG) | Paleocene | 61–58 | Basalt, tuff layers |
| Ulster White Limestone formation (UWLF) | Early | 85–69 | Chalk, some flint |
| Lower Lias Waterloo mudstones (LLG) | Cretaceous | 199–182 | Mudstone, thin limestone |
| Dolerite sills | Paleocene | 61–58 | Dolerite, basalt |
| Mercia Mudstone group (MMG) | Late Triassic | 247–209 | Mudstone, siltstone |
| Lagavarra Formation (LF) | Late Triassic | 247–209 | Sandstone, siltstone, thin mudstone |
| Sherwood Sandstone group (SSG) | Early Triassic | 252–247 | Fine-grained sandstone |
| Belfast group (BG) | Late Permian | 260–252 | Sandstones, claystones, marls |
| Enler group (EG) | Early Permian | 290–272 | Fine-grained sandstone |

depth within the Rathlin Basin (Wilson and Manning, 1978). Based on modelling of the then-available gravity data, the borehole was predicted to intersect Carboniferous lithologies at a depth of ≈ 1500 m. However, a succession of dolerite sills was encountered in the hole (Fig. 3), the elevated density of which had a strong effect on the gravity anomaly used to estimate the expected depths. As a consequence, the Permian and Triassic sediments extend to far greater depth than predicted from the gravity model, and the base of the Permian sequence was not reached by the depth at which drilling terminated due to technical difficulties.

In addition to the lithological sequence itself (Fig. 3), several sets of geophysical data were also acquired from downhole measurements. Gamma ray and neutron porosity data were logged from the surface to

1481 m depth (the base of the borehole was not reached due to technical difficulties), with DC resistivity and self-potential logs also acquired through the Mercia Mudstone and Sherwood Sandstone groups (MMG and SSG, respectively) from 1050 to 1450 m. Equilibrated temperature data were measured in the uppermost 600 m of the borehole, with interval geothermal gradient estimates ranging from 20 K km^{-1} in the Ulster White Limestones to 50 K km^{-1} in the Lower Lias and dolerite sills. Although Wilson and Manning (1978) accounted for paleoclimate effects (Beardmore and Cull, 2001), due to the shallow depths of temperature measurement these geothermal gradients shed little insight on the deeper formations of interest.

4.1.1. DC resistivity log

DC resistivity wireline logs sample the near-hole resistivity distribution of the borehole over the length of a “sonde”, the downhole tool, producing resistivity data at a resolution far greater than achievable by MT or any other surface electrical or electromagnetic geophysics (Ellis and Singer, 2008), but sampling only a small volume ($< 1 \text{ m}$) around the borehole, whereas MT and other EM methods produce a volumetrically integrated average from the surface to the depth of interest. The resistivity log was acquired over the depth interval from 1050 to 1450 m in the PM1 borehole (denoted by vertical black bar in Fig. 3), which covers the lower portion of the Mercia Mudstone group (MMG) and the upper portion of the Sherwood Sandstone group (SSG). The resistivity data are plotted in Fig. 4 (left column). Although the data are highly variable within each formation, reflecting the highly localised sampling of heterogeneous material, clear differences between the formation samples are evident. Furthermore, the 95 m thick Lagavarra Formation (LF), which forms the base of the MMG, comprises a mix of sandstone and mudstone layers, and by treating this formation as a separate unit the resistivity differences remain. Histograms of each of these sample groups are also shown in Fig. 4 (right column), as are the respective logarithmic median resistivities of $3.2 \Omega\text{m}$ (MMG), $4.8 \Omega\text{m}$ (LF), and $6.2 \Omega\text{m}$ (SSG).

Although downhole resistivity tools and MT each give information about the resistivity of the Earth, the two methods rarely return the same information due to differences in sampling methodologies and underlying physics. Downhole tools typically observe resistance to near-vertical DC currents across distances $< 1 \text{ m}$, whereas the MT method infers resistance to inductive (time-varying), near-horizontal electric fields over distance scales of the depths of interest, typically tens to thousands of metres. In addition to the difference in scale, the orientation of the electric fields can also play a part due to electrical anisotropy within the media themselves. As a result, for the purposes of MT modelling the borehole resistivity measurements are limited to that of supporting qualitative information on the relative resistivities of the sediments.

4.1.2. Neutron porosity log

The neutron porosity log measures the absorption of emitted neutrons by the rock formation, and is strongly sensitive to the presence of hydrogen – typically, the presence of clays, shales, or formation waters in pore spaces. As high concentrations of hydrogen are found in multiple different forms, older neutron porosity data are reported in American Petroleum Institute (API) units rather than a percentage porosity (Scott, 1984). It should be noted that an increase in API units of neutron porosity corresponds with a *decrease* in hydrogen content (i.e. a decrease in neutron porosity indicates an increase in clay, shale, water or oil content of the formation).

Fig. 5(left column) shows the neutron porosities (in orange) and electrical resistivities (in blue) observed in the PM1 borehole across the sedimentary units of interest. Normalised correlations between these quantities are also shown for the MMG, LF and SSG, with a correlation of 1 indicating that resistivity and neutron porosity fluctuate in unison with the specified lag. This is exemplified by the cross-correlations of the MMG and SSG, each of which spikes to ≈ 0.8 with zero lag. As there

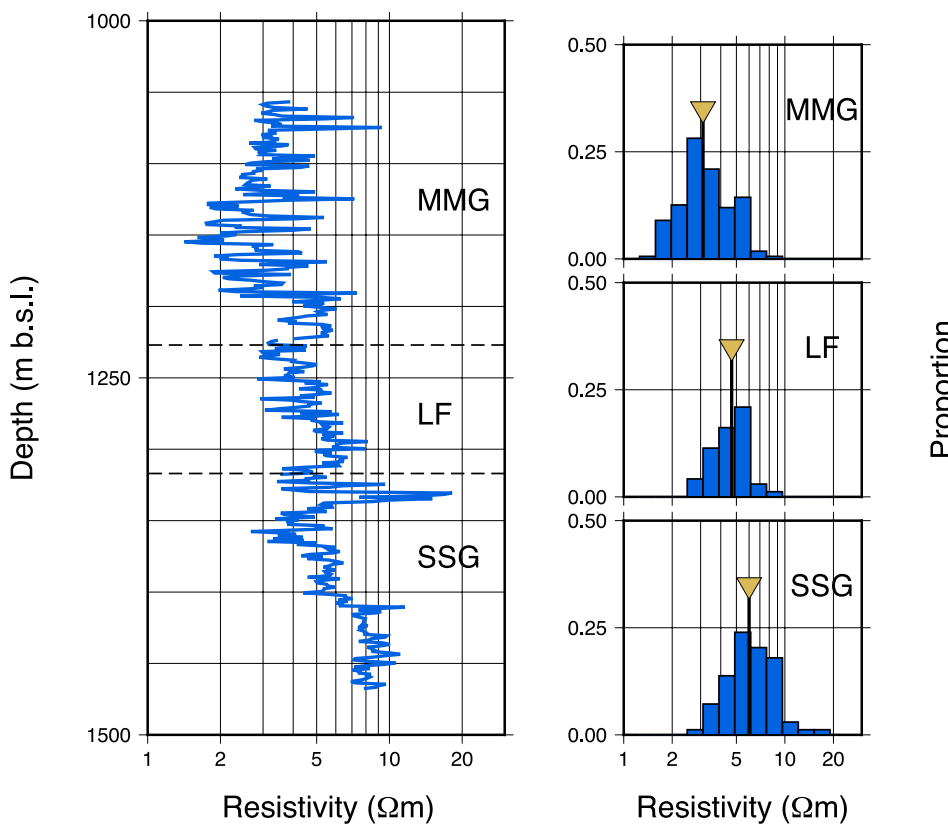


Fig. 4. Left-hand subfigure shows measured resistivity data with depth from 1050 to 1450 m in PM1 borehole, sampling from the Mercia Mudstone group (MMG) into the underlying Sherwood Sandstone group (SSG). The basal Lagavarra Formation (LF) within the MMG is also labelled. The MMG and LF formations are relatively consistent in their resistivities, with a slight increase in resistivity below 1150 m, whereas the SSG tends to continue to increase in resistivity. In order to examine further the increase in resistivity with depth, the log-resistivity distributions from each of the three units are shown in the right-hand subfigures. Given the differences in central tendency of each formation, the units can be assumed to have distinct median resistivities (marked by vertical black line with yellow triangles). (For interpretation of the references to colour in this figure legend, the reader is referred to the web version of the article.)

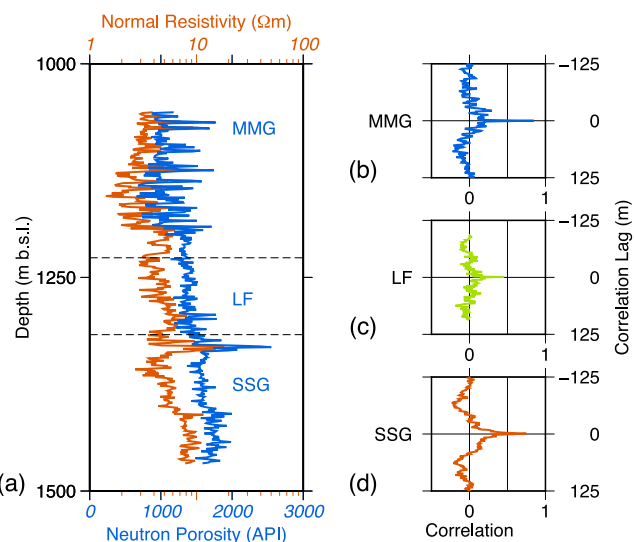


Fig. 5. Left-hand subfigure shows the measured neutron porosity (in American Petroleum Institute – API – units) in blue, and the measure wireline resistivities in orange from the deeper section of the PM1 borehole. Note that neutron porosity data when presented in API units has a negative correlation with true percentage porosity. The right-hand subfigures show the normalised correlation between the neutron porosity and resistivity in each of the three formations marked (i.e. MMG, LF, and SSG), where a correlation of 1 describes two data sets that fluctuate in perfect unison. Both the MMG and SSG show strong correlations between neutron porosity and resistivity, implying that the formations' resistivities are strongly affected by porosity or clay content. The reduced correlation peak amplitude of the LF implies that the properties are more weakly linked, with some other factor influencing one or both of porosity and resistivity.

is a well-documented empirical relationship (Archie's Law) between a sandstone formation's effective porosity and effective resistivity (defined in Archie (1947), discussed at length in Glover (2010), and specifically for relevant Irish lithologies in Campanyà et al. (2015)), the strong positive correlation between neutron porosity (recalling the inverse relationship between neutron porosity and percentage porosity) and resistivity implies that the fluid content of pore spaces has a lower resistivity than the surrounding sandstone or mudstone matrix. As the MMG formation is known to have generally poorer hydraulic properties we interpret the strong correlation between MMG neutron porosity and resistivity as indicative of elevated clay content, whereas for the known porous and permeable SSG unit we interpret the correlation as indicative of elevated porosity or permeability.

4.1.3. Laboratory porosity and permeability measurements

Laboratory measurements of porosity and hydraulic permeability taken from SSG core samples from the PM1 borehole are presented in Wilson and Manning (1978). The measured porosities and hydraulic permeabilities are plotted in Fig. 6, colour coded by the depth at which the respective samples were recovered. Note that the permeability measurements were corrected for Klinkenberg effects, i.e. corrections have been applied to compensate for viscosity and density differences between the gas used in laboratory measurements and the expected pore fluids. Klinkenberg correction also accounts for the Klinkenberg effect, where in low flow (i.e. low permeability) situations a gas will not encounter the same boundary effects within pores as a liquid (Klinkenberg, 1941). The change in relationship between porosity and log-permeability above moderate permeabilities (i.e. $\Phi > 18\%$) is typical of clastic rocks, and arises from the development of sufficient flow velocities so as to create boundary layers within the flow paths that impede some of the flow (Chilingarian and Wolf, 1975; Bernabe et al., 2003).

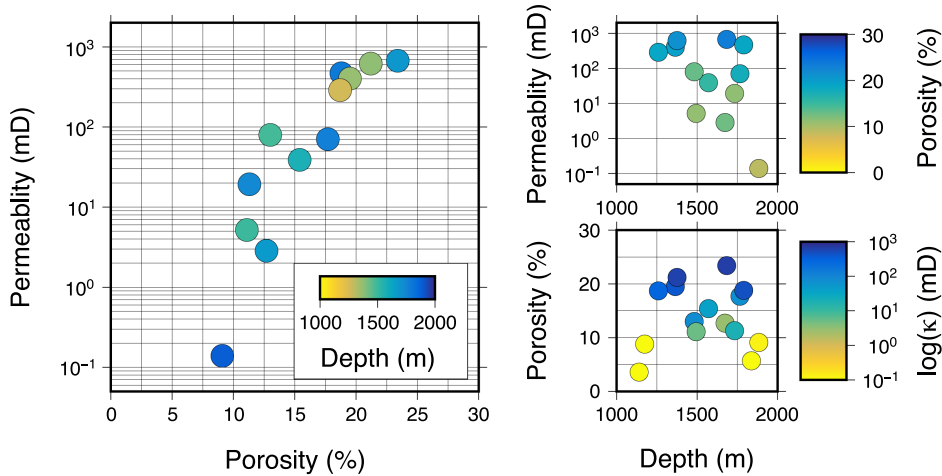


figure legend, the reader is referred to the web version of the article.)

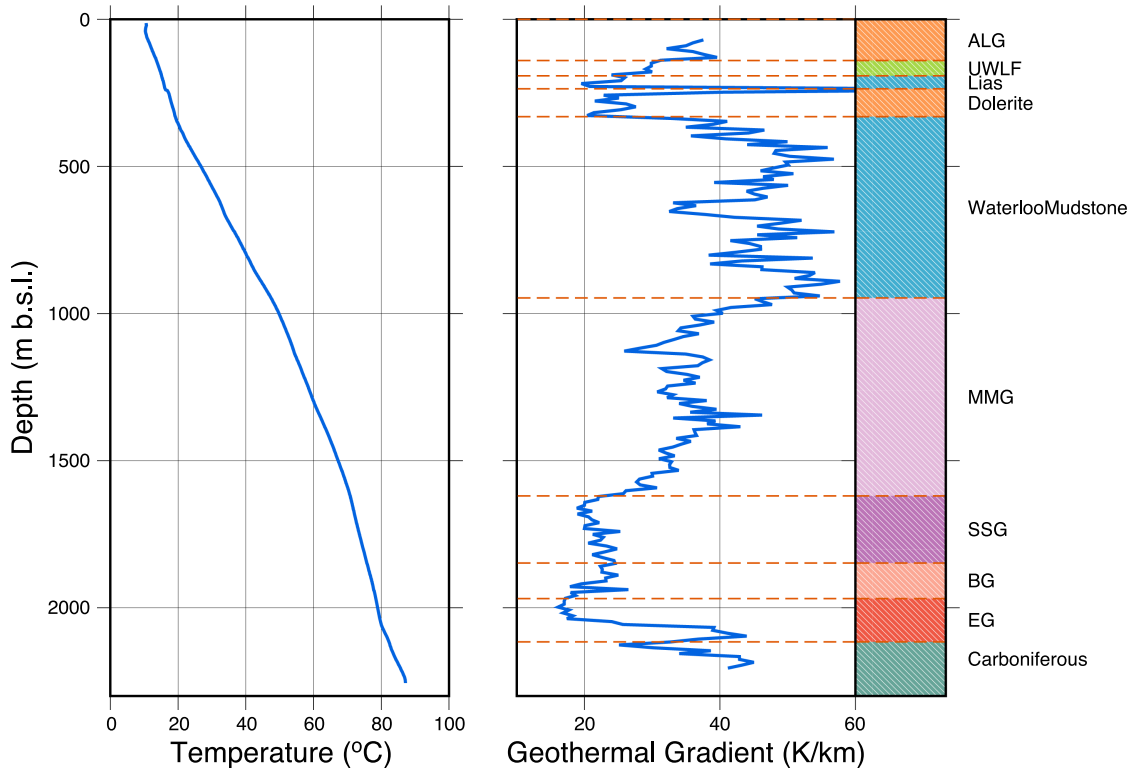


Fig. 7. Left-hand panel shows observed temperatures (blue) with depth in the B1 borehole. Observed data were measured in 2015, with sufficient post-drilling time (≈ 7 years) that the temperatures are assumed to be in thermal equilibrium with the surrounding formations. Central panel shows first difference of the temperature data, giving estimates of the geothermal gradient within each formation (assumed to be approximately constant for a unit with “homogeneous” thermal conductivity). Right panel shows formations observed in the B1 borehole. (For interpretation of the references to colour in this figure legend, the reader is referred to the web version of the article.)

4.2. Ballinlea-1 borehole

Equilibrated temperature measurements in the B1 borehole on behalf of Rathlin Energy (UK) Ltd., confirm the elevated temperatures previously reported within the basin, shown in Fig. 7. The temperature data allow estimation of geothermal gradients by piecewise divided differences (i.e. approximating the first vertical derivative of temperature). The relationship between temperature gradients ∇T (geothermal gradients in this case, in km^{-1}), thermal conductivity λ ($\text{W m}^{-1}\text{K}^{-1}$), and heat flux density Q (in this case, assumed to be near-vertical, W m^{-2}), is described by Fourier's Law, given as Eq. (1),

$$Q = -\lambda \nabla T. \quad (1)$$

The thermal conductivity of a lithological unit is primarily dependent on its quartz content and porosity. Provided that there is no significant advective fluid flow, interval geothermal gradient estimates can be taken as a proxy for the inverse of the lithological unit's thermal conductivity. It should be noted that the relationship between thermal conductivity and geothermal gradient can be biased by lingering paleoclimate effects on the temperature field (Beardmore and Cull, 2001; Bodri and Cermak, 2007), however, as the target sediments occur at depths greater than 1 km the paleoclimate effect is likely small (i.e., $< 5 \text{ mW m}^{-2}$ change in heat flow density). As long as adjacent

formations have contrasting thermal conductivities, variations in geothermal gradient estimate should be consistent with the formation boundaries. Such a comparison for the observed B1 temperature measurements is shown in Fig. 7, although visually some of the formations are thermally indistinct from one another at this scale (i.e. the Lower Lias, MMG and any intermediate dolerite sills). In particular, the SSG and BG formations are thermally indistinct (i.e., the units have very comparable geothermal gradients of $\approx 24 \text{ K km}^{-1}$), as they have similar composition and porosities. However, the deeper, Permian EG formation has a decreased geothermal gradient in comparison to the BG formation. Assuming a constant heat flux, the decrease in geothermal gradient from the BG to EG units suggests a corresponding increase in thermal conductivity, likely due to a decrease in either clay content or porosity in the EG (when compared to the BG), or an increase in quartz content in the EG.

5. Magnetotelluric exploration

The magnetotelluric (MT) method is a geophysical technique that images subsurface electrical resistivity structure by examining the attenuation of electromagnetic (EM) waves within the Earth, and is well described in e.g., Chave and Jones (2012). At the frequencies of the MT method, this attenuation through a body of rock is dependent upon three factors, namely, the frequency of the wave, the electrical resistivity of the rock volume, and the magnetic permeability of the rock volume (generally, insignificantly different to that of free space, although at high frequencies over granitic plutons one must consider magnetic permeability, e.g., Kao and Orr (1982, 1982)). Hence, sampling EM waves with a range of frequencies allows for the derivation of an electrical resistivity model that reproduces the observed MT responses. The electrical resistivity of a volume of Earth material is sensitive to a wide range of factors, including mineral composition, alteration, temperature, and the presence and distribution of fluids. In particular, for the purpose of evaluating the Rathlin Basin as a possible geothermal aquifer, it was expected that the presence of saline geothermal waters in the elevated porosities of the Permian and Triassic sandstones would be manifest as elevated observed electrical conductivities (equivalently, a reduction in observed electrical resistivity).

MT data were acquired over half of the onshore basin area that includes the two boreholes in order to extend understanding of basin structure beyond the two boreholes and mapped geophysical data. MT data were acquired at a total of 39 sites north-west of the bounding Tow Valley Fault (TVF), at locations shown in Fig. 2. In addition to correction of static-shift type distortion in the MT data, Delhaye et al. (2017) also presents the results of dimensionality analysis by use of the *strike* analysis tool (McNeice and Jones, 2001), implying approximately 1D resistivity structure within the uppermost 3000 m. Although 3D inverse models of the Rathlin Basin MT data are presented in Delhaye et al. (2017), they have been disregarded in favour of 1D inversion of invariant data for this work. This judgement is based primarily upon the sub-optimal acquisition site spacings with respect to the geological targets of interest and general resistivity trends. As the majority of resistivity structure resolved in the 3D models of Delhaye et al. (2017) are within the uppermost 2 km, a large proportion of resolved structure is within the inductive region of only a single site. The advantages of 3D inversion in modelling lateral resistivity structure cannot be fully exploited without overlapping data coverage from adjacent sites, resulting in a “3D resistivity model” that consists of effectively independent models of each site's data interpolated between sites by the inversion algorithm. Given the 1D resistivity structure indicated by dimensionality analysis, it is reasonable to invert the computed 1D data in a strictly 1D sense, and interpolate these models separately, although interpretation is limited to horizontal boundaries. Identifying lateral resistivity structure at scale lengths smaller than the MT site spacings is not feasible based upon the work presented here. The main issue with interpreting pseudo-3D models based upon interpolation of 1D models

is the effect of static shift-type distortion, however, in our case such static-shift effects have been addressed (Delhaye et al., 2017).

Monte Carlo inversion of MT data was proposed in 1979 by Jones and Hutton (1979), and has advanced since then. Transdimensional Markov Chain Monte Carlo approaches (MCMC hereafter) have been proposed by several authors (Brodie and Jiang, 2018; Mandolesi et al., 2018) as a means to explore the non-uniqueness and range of plausible 1D inverse models. For sufficiently long Markov chains the ensemble will approximate the posterior probability density (PPD) of the true resistivity-depth model, and conclusions can be drawn about the likelihood of certain model features. Transdimensional implementations of MCMC modelling include the dimensionality of the problem (i.e., the number of layers) as an additional simulated parameter (Green, 1995). For investigation of the Rathlin Basin MT data, four chains of 10 million (i.e., 10^7) models were computed with the reversible-jump MCMC code of Brodie and Jiang (2018) for each MT site. Model ensembles were computed for invariant MT data (i.e., the geometric mean of apparent resistivities, and arithmetic mean of phases) with assumed error floors of 5% (ρ_a) and 2° (ϕ), with models defined by a domain of depth bins ranging to 5000 m depth. Misfits of models are defined in a standard chi-squared manner (Eq. (2)). This formulation of misfit assumes that the errors ε_i are normally distributed, and hence a misfit equal to the number of data implies that the average datum is reproduced with a residual equal to the error. We note that the assumptions of misfit are inherently violated by the application of an error floor, however, it remains a useful measure of the progression of the Markov chain as it clearly visualises when the chains converge to a region of model space of minimal misfit.

$$\delta(m) = \sum_{i=1}^N \left(\frac{d_i - d_r}{\varepsilon_i} \right)^2. \quad (2)$$

The complete results and model ensemble parameters for each MT site can be found in the supplementary material. To illustrate the format and interpretation of the ensembles, we present the respective ensembles for the two sites adjacent to the PM1 and B1 boreholes. Each ensemble is presented in a similar manner, with the input and invariant data plotted against a best-fitting model's responses, a histogram of the number of layers in each model within the ensemble, and a plot of the misfit progression of the model chain. The posterior probability density function (PDF) of the resistivity and depth distribution of the ensemble is plotted, normalised by the mode of each depth bin to highlight modal behaviours of the ensemble, with statistical measures overlain. Finally, interpreted formations and any comparative information are displayed for each site. Model ensembles have been interpreted on a formation basis by considering primarily the modes and medians of each ensemble, with means and 10th-percentiles used in some cases. The 90th-percentile line is less useful as modelled resistivities tend to be virtually unbounded at the resistive end of the spectrum than at the conductive end, as evident by the skewed distribution of 10th- and 90th-percentile lines with respect to medians (by definition, the 50th-percentile line). This is due to induction studies being sensitive to the integrated conductivity of conductive layers and insensitive to the actual resistivity of resistive layers, save for defining a minimum bound (see, e.g., Jones (1999)).

Figs. 8 and 9 display the model ensembles for the sites adjacent to the PM1 and B1 boreholes, with the respective formation logs (note that surficial basalts are implied, and not explicitly interpreted). Note that as neither ensemble clearly resolves the top of the EG formation, the encountered depths from boreholes have been included to aid later interpolation. Both ensembles have interpretations generally consistent with the borehole formation log, with the exception of the intrusive dolerite sill intercepted in the PM1 borehole (and the aforementioned EG boundary). Due to the possibly extreme resistivity contrasts between the highly conductive LLG sediments and the igneous sills, clear interpretation of similar sills is difficult across the basin, as although some

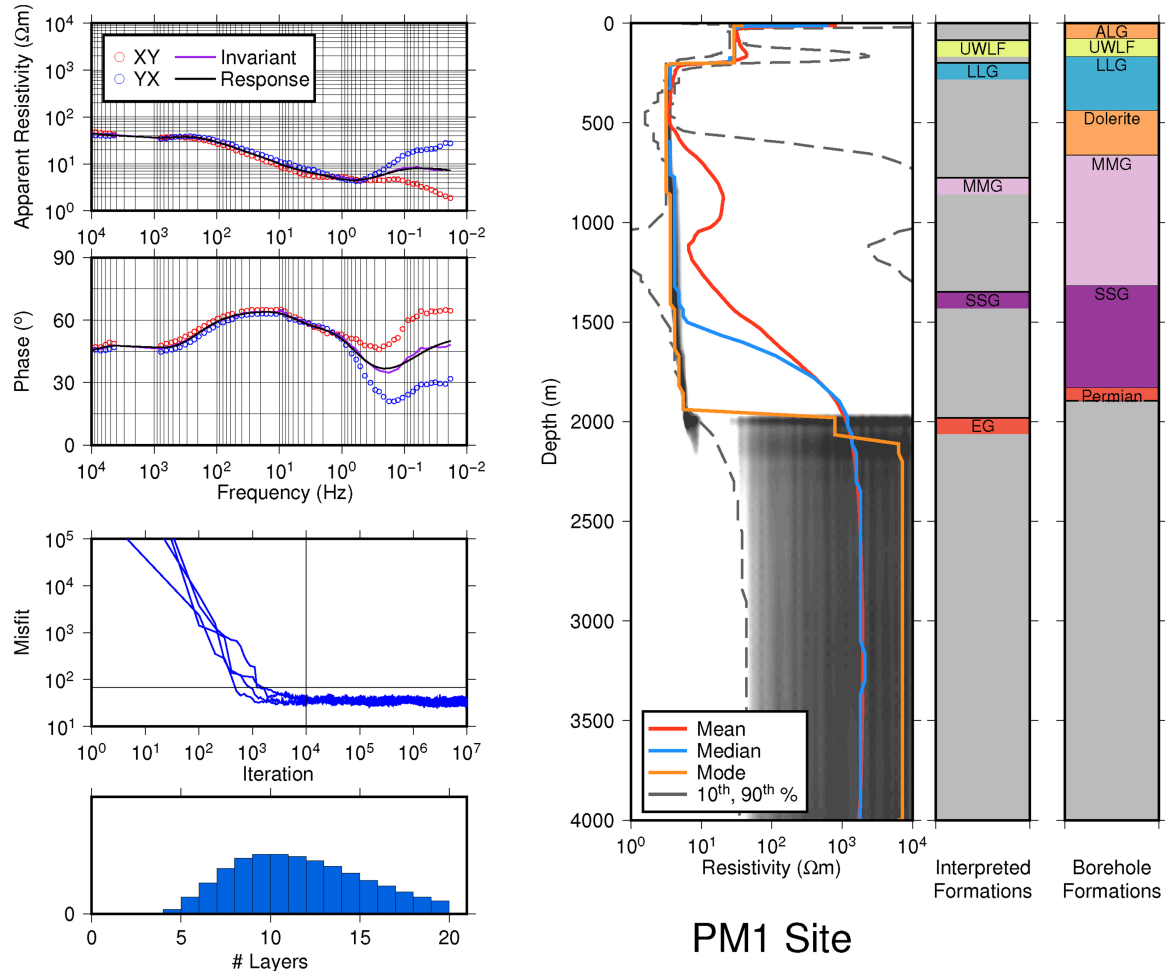


Fig. 8. Display of MCMC model ensemble for site adjacent to the PM1 borehole. Left column includes plots of data and model responses, misfit progression for MCMC chain (with 10 000 burn-in chain and ideal misfit marked), and histogram of number of layers in the ensemble models. Central plot shows a shaded heatmap of the logarithmic PPD of the model density, normalised by the mode of each depth bin. Statistical measures of the ensemble are overlaid on the heatmap. Right columns show the formation tops as interpreted from the ensemble, compared to the formation sequence observed in the PM1 borehole (as shown in Fig. 3).

ensembles feature distinct resistive bands with similar appearances to the dolerite sill in the B1 borehole, it remains possible that further sills are concealed within the formations of other ensembles. The igneous intrusions appear limited to Jurassic and younger formations, however, and hence are not considered further for the interpretation of the target sediments (i.e., the SSG and BG sediments).

Based upon the comparison between ensemble interpretations and borehole formation logs, and continuity of formation depths and thickness between adjacent ensemble interpretations, we consider that the interpreted SSG reservoir thicknesses are sufficiently precise for the purposes of an order-of-magnitude geothermal resource estimation. Fig. 10 presents interpolated surfaces corresponding to the interpreted tops of the MMG, SSG, and EG units, with the EG assumed as the base of a potential reservoir, and the thickness distribution for the combined SSG and BG reservoir volume is presented in Fig. 11. For the purpose of quantitative geothermal resource estimation we have truncated the assumed reservoir extent based upon the EG interpretation, resulting in an assumed reservoir of thickness between 100 m and 400 m, with a total volume of 32 km³.

6. Indicated geothermal reserve estimation

From existing knowledge of the Rathlin Basin and new insights gained from the MT resistivity models presented here, it is possible to classify the Rathlin Basin as an Indicated Geothermal Reserve [as

defined in Lawless (2010)] by estimating the exploitable volume of reservoir rocks V , and in turn the thermal energy in place Q_{th} . Note that precise quantification of the geothermal prospects in the Rathlin Basin is difficult due to limited information on thermal and hydraulic properties; regardless, by appropriate assumptions an order-of-magnitude estimate of the heat in place can be made.

The method of estimation used here follows that presented in Lawless (2010) for estimating Q_{th} as a function of temperature change ($T_i - T_f$) and porosity, as shown in Eq. (3):

$$Q_{th} = V \times \{[(C_r \rho_r (1 - \Phi)(T_i - T_f)] + [C_w \rho_w \Phi(T_i - T_f)]\} \quad (3)$$

In this equation, C_w is the specific heat capacity of water, assumed constant at 4181 J kg⁻¹ C⁻¹, and C_r is the specific heat capacity of the rock matrix, taken as 816 J kg⁻¹ C⁻¹ for a similar Permian sandstone in the UK (Richardson and Neymeyer, 2013). The porosity Φ was taken as $14 \pm 1.5\%$, i.e. the mean of the laboratory measurements shown in Fig. 6. The density of the rock matrix, ρ_r was taken as 2450 ± 50 kg m⁻³ (Mitchell, 2004), whereas the density of water ρ_w was treated as a function of temperature [as defined in Adams and Bachu (2002)]. As the two target formations (i.e. the SSG and BG sandstones) have the same observed geothermal gradient (≈ 24 K km⁻¹, from Fig. 7), for geothermal estimation purposes they can reasonably be treated as a single unit, with a range of initial temperatures T_i linearly interpolated from the appropriate section of observed temperature measurements shown in Fig. 7.

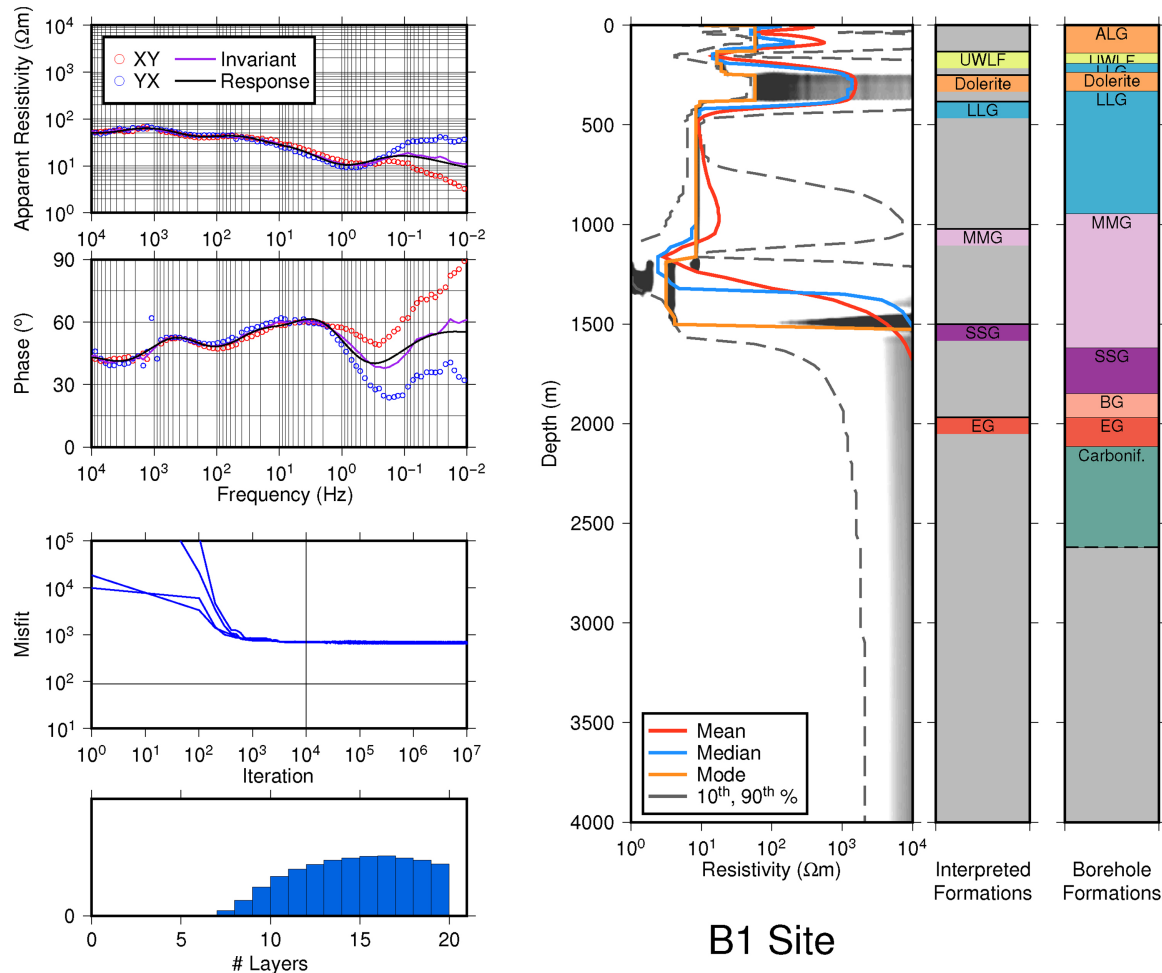


Fig. 9. Display of MCMC model ensemble for site adjacent to the B1 borehole. Left column includes plots of data and model responses, misfit progression for MCMC chain (with 10 000 burn-in chain and ideal misfit marked), and histogram of number of layers in the ensemble models. Central plot shows a shaded heatmap of the logarithmic PPD of the model density, normalised by the mode of each depth bin. Statistical measures of the ensemble are overlaid on the heatmap. Right columns show the formation tops as interpreted from the ensemble, compared to the formation sequence observed in the B1 borehole (as shown in Fig. 7).

The formation depths interpreted in the previous section were interpolated over an appropriate portion of the survey area to estimate the total volume for the target SSG and BG sediments, and uncertainties of 20 m were attributed to the depths of each boundary. As the Dalradian horst south-east of the TVF represents a significant volume of non-sedimentary material at depth due to its sub-vertical dip between 25° and 56° to the north-west [modelled from gravity data by Gibson (2004)], this volume must be accounted for to avoid overestimating the sediment volume. The TVF was assumed to be planar with a dip of 40° [the mean dip reported by Gibson (2004)], resulting in a triangular prism that models the displacement of sediments at depth. The volume of the triangular prism was then subtracted from the total sediment volume to approximate the absence of sediments due to fault loss adjacent to the TVF. Finally, the reservoir volume was fractionally adjusted to compensate for the discrepancy between the formation-level interpretation and lithology-level reality; as a significant fraction of the SSG interpreted in the PM1 borehole is conglomerate rather than sandstone, it would be inappropriate to neglect that such conglomerate is less likely to contribute to a reservoir. Based upon the thicknesses of conglomerate and sandstone encountered in the PM1 borehole (i.e., 148 m of conglomerate in the 579 m thick SSG interval), the volume presented previously in Fig. 10 was reduced by a further 25% to account for the viable proportion of the reservoir (note that in reality the SSG-BG interval likely represents several smaller reservoirs due to conglomerates acting as barriers to permeability).

Final reservoir temperatures T_f were varied from 85 °C down to 25 °C, and the results with error estimates (typically $\approx \pm 30\%$) are plotted in Fig. 12, in the left-hand panel. The lower boundary of $T_f = 25$ °C was selected to facilitate comparison with existing estimates of geothermal potential in the adjacent Larne basin (Pasquali et al., 2010; Busby, 2014). The stored heat in place Q_{th} increases as the final temperature decreases, an expected result as the volume of viable (i.e. at a temperature greater than T_f) reservoir rocks increases. The non-linearity of Q_{th} for small $(T_i - T_f)$ arises as only a small amount of the reservoir has a sufficiently high initial temperature T_i ; as $(T_i - T_f)$ increases, more of the reservoir is usable, and Q_{th} rises due to the increases in both V and $(T_i - T_f)$. Modelling of the Rathlin Basin for a $T_f = 25$ °C gives an estimated Q_{th} of 2900 ± 600 PJ for the assumed geothermal reserve; to place this Q_{th} estimate in context, the nearby Larne Basin has been estimated to have $Q_{th} = 1800$ PJ in place for the same T_f (Pasquali et al., 2010; Busby, 2014).

A comparison of the volume exploited V , and the rate of change $\partial V / \partial T_f$, to the final temperature T_f is shown in Fig. 13. As seen by the change in volume with respect to T_f , a target T_f of 55 °C is required to exploit the entire assumed reservoir volume. Exploitation beyond this T_f returns increasing Q_{th} as a linear function of T_f , without the exponential increase due to increasing reservoir volume, and this diminishing returns may limit geothermal exploitation. The geographic distribution of Q_{th} as estimated for $T_f = 25$ °C is presented in Fig. 14, with elevated densities of Q_{th} centrally and to the east of the survey area due to thicker sediments in these areas.

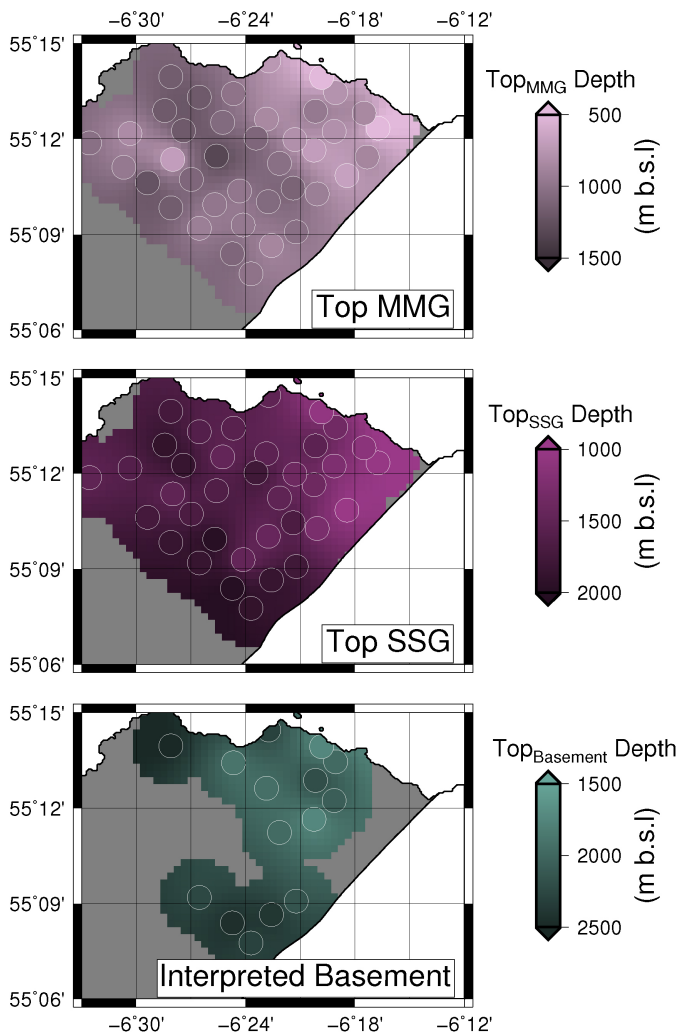


Fig. 10. Depth distributions of the three stratigraphic horizons of principal interest, namely, the tops of the Mercia Mudstone group (MMG), Sherwood Sandstone group (SSG), and the Enner Group of Permian sandstones (EG). White circles mark locations where the boundary was identifiable. The horizons are masked by grey in regions greater than 2 km from an MT site with an identifiable corresponding boundary, to clarify the resolution extent.

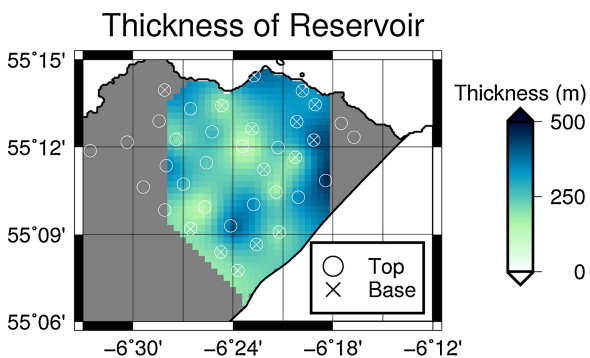


Fig. 11. Distribution of assumed Sherwood Sandstone Group reservoir formation, interpreted from Fig. 10, where ‘Top’ markers are the locations of resistivity models at which Top SSG can be interpreted. Similarly, ‘Base’ markers denote locations of resistivity models at which Top EG can be interpreted. After truncating the volume adjacent to the TVF to compensate for the subvertical basin boundary, the assumed reservoir has a volume of 32 km³.

7. Implications and discussion

At the time of MT data acquisition, existing geophysical models (Mitchell, 2004; Naylor and Shannon, 2011) suggested a depth to the base of Permian sandstones of up to 4000 m, with the PM1 resistivity measurements indicated that the MMG is more conductive than the underlying SSG and BG sandstones. Resistivity measurements from the PM1 borehole suggest that the general resistivity contrasts between the MMG and underlying SSG & BG formations are minor (i.e., a resistivity contrast of 0.3 in log₁₀ units). However, the results of this work indicate that the MMG found within the Rathlin Basin is slightly more resistive when modelled by MT data, and the basin as a whole, or at least the permeable (conductive) parts of the basin, is shallower than predicted. Resistivity models from inversion of MT data sets adjacent to the two deep boreholes can be interpreted into structures comparable to bore-hole knowledge, however, as the data from some of the MT sites have poor signal quality, recovery of the low-resistivity contrast boundaries of interest was not possible at all sites. Additionally, as the MT method is unable to resolve accurately the actual resistivity of a resistive formation beneath a conductor, but only set a minimum value on it, we also cannot be certain that the resistivities estimated for the SSG and BG are sufficiently accurate for porosity estimation.

A major consequence of the shallow, conductive resistivity structure is that due to the nominal 2 km MT site spacing, most of the resistivity structure modelled in the survey area relies upon single MT sites. As a result, we limited the modelling to 1D inversion to avoid interpretation of shallow (i.e. < 1500 m) resistivity structure between MT sites that will, in all likelihood, be more controlled by the smoothing terms of 3D inversion modelling objective function rather than the fit to the data themselves, given by the misfit term in the objective function. However, limiting the modelling to 1D inversion may be less appropriate for longer period MT data, as previous work has shown such data to have characteristics indicative of 3D resistivity basement structure (Delhaye et al., 2017).

Given that the survey area covers less than half of the onshore basin, the entire Rathlin Basin presents a significant geothermal resource in comparison to other onshore geothermal resources in Northern Ireland. However, the most significant aspect of a geothermal reservoir after temperature is the network of pathways of fluid migration, i.e., the hydraulic permeability; in the case of clastic rocks such as the SSG or BG, the distribution of hydraulic permeability can vary significantly across a region, greatly altering the viable reservoir volume. As the limited results from core samples shown in Fig. 6 exhibit a large range of permeabilities, it can be inferred that the distribution of permeability within the basin is complex and significant in limiting intra-reservoir flow. Intra-basin faults have been mapped in the Rathlin Basin by other geophysical methods (Gibson, 2004), and these may function as impermeable barriers to flow, compartmentalising and limiting the continuity of the reservoir. Additional porosity and hydraulic permeability data from new boreholes is essential to obtaining more robust, statistical geothermal models, particularly as there have been some concerns raised regarding the appropriateness of Klinkenberg corrections for the SSG in Britain (Bloomfield and Williams, 1995).

The elevated geothermal conditions within the Rathlin Basin, when compared to the remainder of Ireland, are known solely from borehole temperature measurements in the two deep boreholes, and quantitative analysis is only possible from the equilibrated temperature measurements from the B1 borehole. More accurate estimation of both the heat flux distribution and total heat in place of the basin would require further temperature observations in additional boreholes, and ideally laboratory measurements of formation thermal conductivities. Regardless, although computed by a simplistic bulk approach, the estimates of geothermal heat in place presented here show that the Permo-Triassic sediments within the Rathlin Basin represent a large heat resource.

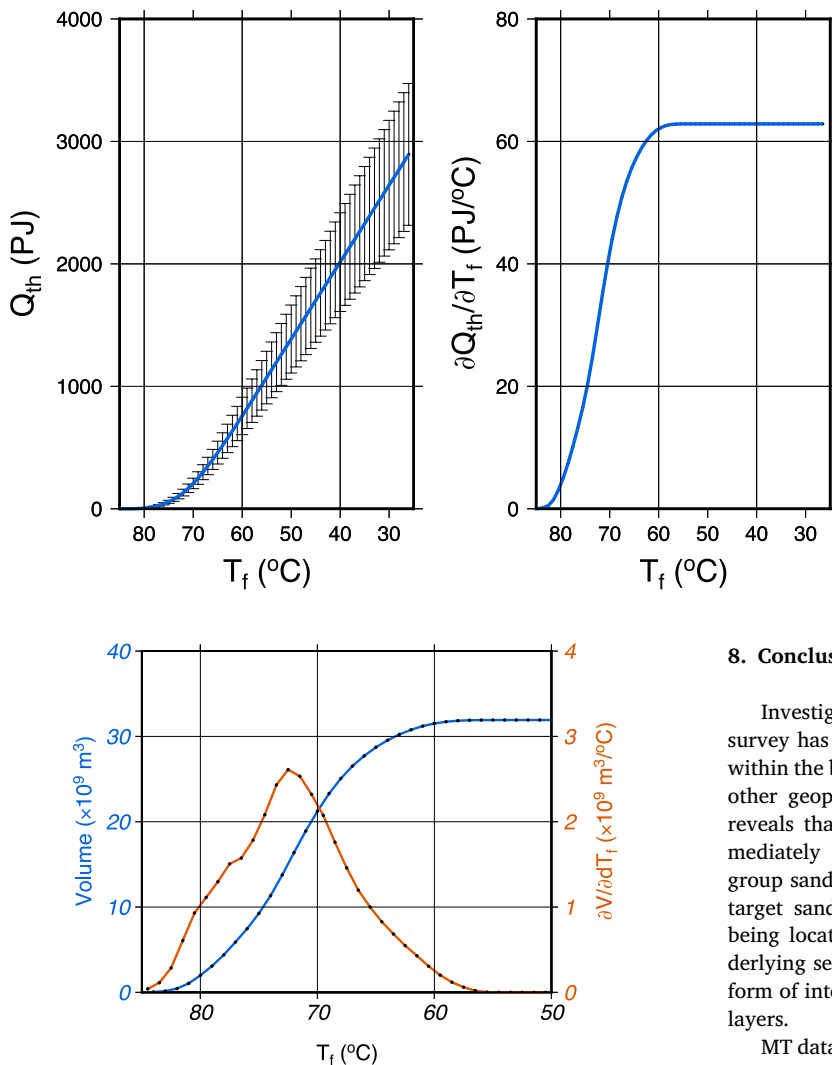


Fig. 13. Diagnostic display of the volume of reservoir sediments at or above the final reservoir temperature T_f (blue), and the increase in reservoir volume with respect to final temperature ($\partial V/\partial T_f$, orange). As temperature is assumed as a linear function of depth, the initial increase in $\partial V/\partial T_f$ from 85 to 73 °C is due to both lateral and vertical (i.e., thickness) expansion of the accessible volume. For $T_f < 73$ °C, $\partial V/\partial T_f$ decreases as the areal extent approaches its limit. In order to maximise exploitation of the reservoir, a target $T_f = 55$ °C is suggested, as exploitation beyond this has diminished thermal energy returns.

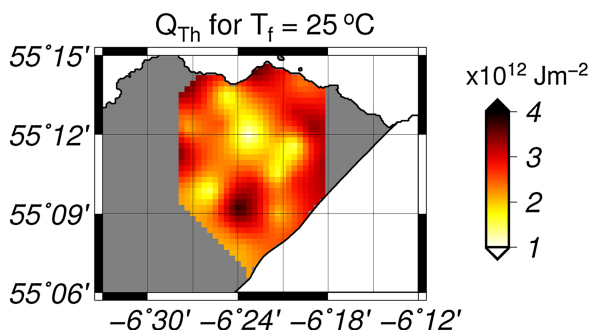


Fig. 14. Geographic distribution of areal density of geothermal energy in place Q_{th} , as computed for $T_f = 25$ °C. The density of geothermal energy in place is elevated towards the centre and eastern portions of the research area, where the reservoir sediment thicknesses are elevated compared to the remainder of the basin.

Fig. 12. Visualisation of the thermal energy in place available as a function of final reservoir temperature, following the approach detailed in Lawless (2010). Left-hand panel shows the thermal energy Q_{th} and uncertainty (typically $\pm 30\%$) in petajoules (i.e. $\times 10^{15}$ J) versus final temperature T_f , and right-hand panel shows the change of Q_{th} with decreasing T_f . Reducing T_f always corresponds to an increase in Q_{th} ; however, as can be seen from the gradient plot on the right the relationship is non-linear until T_f is sufficiently low to allow exploitation of the full volume, i.e. for $T_f < 50$ °C.

8. Conclusions

Investigation of the onshore Rathlin Basin by means of an MT survey has expanded understanding of reservoir sediment distribution within the basin well beyond that previously known from boreholes and other geophysical data. Careful modelling of the observed MT data reveals that a portion of the Mercia Mudstone group (the layer immediately above the target Sherwood Sandstone group and Belfast group sandstones) is more electrically conductive than the underlying target sandstones. Due to the resistivity configuration of the target being located below a conductor, the resistivity estimates of the underlying sediments cannot be relied upon to be accurate, and another form of interpretation was required to distinguish between lithological layers.

MT data were inverted in a reversible-jump MCMC manner, with the resulting model ensembles interpreted on a formation basis. Interpretations of the model ensembles compare favourably to adjacent deep boreholes, and hence formation interfaces were interpolated between the MT sites to form layer boundary estimates across the area. A conservative volume estimate of 32 km³ of target SSG and BG sandstones was computed from the interpolated boundaries, corresponding with the area where both the top SSG and top Carboniferous lithological boundaries were successfully defined.

Estimation of thermal energy in place as a function of final reservoir temperature T_f suggest an Indicated Geothermal Resource of $\approx 2.9 \times 10^{18}$ J (i.e. 2900 PJ) for a final temperature of 25 °C, with the majority of BG and SSG sandstones engaged by final temperature approaching 50 °C. This estimated resource places the Rathlin Basin as a greater IGR than adjacent contemporaneous basins. However, at this stage we are limited to estimating an Indicated Geothermal Resource by the scarce boreholes and geophysical information available; consideration of the Rathlin Basin as a Measured Geothermal Resource would require additional geophysical, geological and temperature information.

Acknowledgements

This work was supported by Science Foundation of Ireland [grant 10/IN.1/I3022 awarded to AGJ], as part of the IREtherm project. MT data acquisition was only possible with the assistance of the IREtherm

MT Team (S. Blake, T. Farrell, C. Hogg, J. Vozar, C. Yeomans). Rathlin Energy (UK) Ltd. are gratefully thanked for providing temperature and lithological information from the B1 borehole. R. Brodie (Geoscience

Australia) is thanked for making the rjMCMC 1D inversion code available for use. We thank an anonymous reviewer for comments and suggestions that improved the manuscript.

Appendix A. Examination of 1D MT model boundary tolerances

As a measure of uncertainty in the assumed boundary depths for computation of the Indicated Geothermal Resource within the Rathlin Basin, synthetic 1D forward testing has been performed for a typical 1D resistivity model. To enable such testing, MT models determined by Occam inversion were reduced from 45 layers to $\approx 7\text{--}8$ layers by use of the layered 1D inversion tool in WinGLink [an implementation of *minim*, Fischer and Le Quang (1981)], wherein layer thicknesses as interpreted from the vertical derivative of *log* were fixed, and best-fitting interval resistivities determined by the inversion. A comparison of the Occam inverse model and corresponding *minim* model at the PM1 borehole site is shown in Fig. 15. Note that replication of the observed MT data by the responses of the *minim* model is not the intent of the comparison being carried out, rather, only the effect of perturbing the boundary depth on a model's response is of interest.

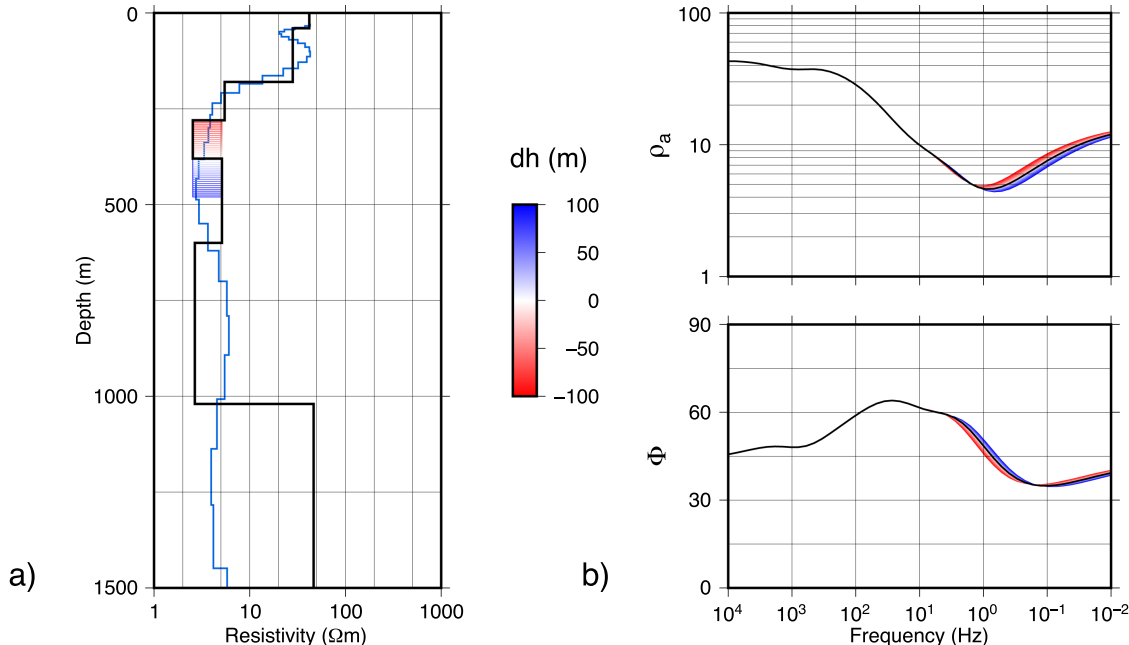


Fig. 15. (a) Comparison of original Occam inverse model (blue line) with *minim* model (black line), and *minim* model perturbed with shifts dh to boundary (red-to-blue lines). (b) 1D MT forward responses of *minim* model (black line) and dh -perturbed models (red-to-blue lines). (For interpretation of the references to colour in this figure legend, the reader is referred to the web version of the article.)

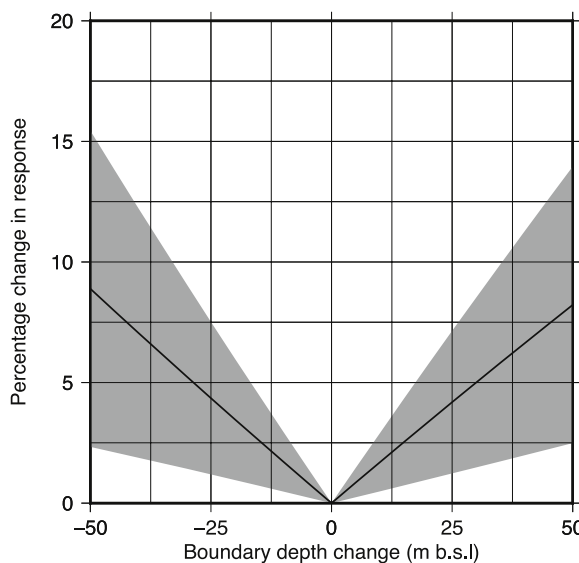


Fig. 16. Plot of total percentage changes in 1D model MT responses as a function of dh change in SSG boundary depth. The mean percentage change of all models is shown by the black line, and the grey region represents one standard deviation. In order to ensure a maximum of 5% change in response (hence, uncertainty of boundary depth) for each model, a tolerance of $\approx \pm 20$ m is required.

The depth of the boundary interpreted as the top of the SSG interval in the *minim* model was perturbed slightly by an incremental change dh of up to ± 100 m in order to examine the effect on the forward responses of the altered models, in comparison to the responses of the original *minim* model. A root-mean-square deviation in response (expressed as a percent change) was computed for each dh between -100 m (i.e., shallower boundary depth) and $+100$ m (i.e., deeper boundary depth), and the resulting distribution of deviation as a function of dh was considered. The responses and distribution of percent deviation for the PM1 borehole site are also shown in Fig. 15 as an example of the process. Fig. 16 presents the distribution of percentage deviation for all the sites interpreted in this manner. By considering these results, if a maximum tolerable deviation of 5% of a model's responses is assumed, then dh of up to ± 20 m are possible at the majority of sites.

References

- Adams, J.J., Bachu, S., 2002. Equations of state for basin geofluids: algorithm review and intercomparison for brines. *Geofluids* 2 (4), 257–271.
- Archie, G.E., 1947. Electrical resistivity an aid in core-analysis interpretation. *AAPG Bull.* 31, 350–366. <https://doi.org/10.1306/3d93395c-16b1-11d7-8645000102c1865d>.
- Beardmore, G.R., Cull, J.P., 2001. Crustal Heat Flow: A Guide to Measurement and Modelling. Cambridge University Press.
- Berdichevsky, M., Dmitriev, V., 1976. Distortion of magnetic and electric fields by near-surface lateral inhomogeneities. *Acta Geod. Geophys. Montan. Acad. Sci. Hung.* 11, 447–483.
- Bernabe, Y., Mok, U., Evans, B., 2003. Permeability–porosity relationships in rocks subjected to various evolution processes. *Pure Appl. Geophys.* 160, 937–960.
- Bloomfield, J., Williams, A., 1995. An empirical liquid permeability–gas permeability correlation for use in aquifer properties studies. *Q. J. Eng. Geol. Hydrogeol.* 28 (Supplement 2), S143–S150.
- Bođri, L., Čermák, V., 2007. Borehole Climatology: A New Method How to Reconstruct Climate. Elsevier, Oxford.
- Brodie, R., Jiang, W., 2018. Trans-dimensional Monte Carlo inversion of short period magnetotelluric data for cover thickness estimation. *ASEG Extended Abstracts 2018* (1), 1–7.
- Bullard, E.C., 1947. The time necessary for a bore hole to attain temperature equilibrium. *Geophys. Suppl. Month. Notices R. Astron. Soc.* 5 (5), 127–130. <https://doi.org/10.1111/j.1365-246X.1947.tb00348.x>.
- Busby, J., 2014. Geothermal energy in sedimentary basins in the UK. *Hydrogeol. J.* 22 (1), 129–141.
- Campanyà, J., Jones, A.G., Vozár, J., Rath, V., Blake, S., Delhayé, R., Farrell, T., 2015. Porosity and permeability constraints from electrical resistivity models: examples using magnetotelluric data. In: Proceedings of the World Geothermal Congress 2015. 15–19 April 2015, Melbourne, Australia.
- Chave, A.D., Jones, A.G., 2012. The Magnetotelluric Method Theory and Practice. Cambridge University Press <https://doi.org/10.1017/cbo9781139020138>.
- Chillingarian, G.V., Wolf, K.H., 1975. Compaction of Coarse-grained Sediments, I Vol. 18 Elsevier.
- Delhayé, R., Rath, V., Jones, A.G., Muller, M.R., Reay, D., 2017. Correcting for static shift of magnetotelluric data with airborne electromagnetic measurements: a case study from Rathlin Basin, Northern Ireland. *Solid Earth* 8 (3), 637–660. <https://doi.org/10.5194/se-8-637-2017>.
- Ellis, D.V., Singer, J.M., 2008. Well Logging for Earth Scientists, 2nd ed. Springer, Dordrecht, The Netherlands.
- Fischer, G., Le Quang, B., 1981. Topography and minimization of the standard deviation in one-dimensional magnetotelluric modelling. *Geophys. J. Int.* 67 (2), 279–292.
- Gibson, P.J., 2004. Geophysical characteristics of the Tow Valley Fault Zone in North-East Ireland. *Irish J. Earth Sci.* 22, 1–13.
- Glover, P.W.J., 2010. A generalized Archie's law for n phases. *Geophysics* 75 (6), E247–E265. <https://doi.org/10.1190/1.3509781>.
- Green, P.J., 1995. Reversible jump Markov chain Monte Carlo computation and Bayesian model determination. *Biometrika* 82 (4), 711–732.
- Jones, A., Hutton, R., 1979. A multi-station magnetotelluric study in southern Scotland - ii. Monte-Carlo inversion of the data and its geophysical and tectonic implications. *Geophys. J. R. Astron. Soc.* 56, 351–368.
- Jones, A.G., 1988. Static shift of magnetotelluric data and its removal in a sedimentary basin environment. *Geophysics* 53 (7), 967–978. <https://doi.org/10.1190/1.1442533>.
- Jones, A., 1999. Imaging the continental upper mantle using electromagnetic methods. *Lithos* 48, 57–80.
- Kao, D., Orr, D., 1982. Magnetotelluric response of a uniformly stratified earth containing a magnetized layer. *Geophys. J. Int.* 70 (2), 339–347.
- Klinkenberg, L.J., 1941. The permeability of porous media to liquids and gases. *Drill. Prod. Prac.* 200–213.
- Lawless, J., 2010. Geothermal Lexicon for Resources and Reserves Definition and Reporting. Australian Geothermal Energy Group.
- Mandolesi, E., Ogaya, X., Campanyà, J., Agostinetti, N.P., 2018. A reversible-jump Markov chain Monte Carlo algorithm for 1D inversion of magnetotelluric data. *Computers Geosci.* 113, 94–105.
- McNeice, G.W., Jones, A.G., 2001. Multisite, multifrequency tensor decomposition of magnetotelluric data. *Geophysics* 66 (1), 158–173. <https://doi.org/10.1190/1.444291>.
- Mitchell, W.I., 2004. The Geology of Northern Ireland: Our Natural Foundation. Geological Survey of Northern Ireland, Belfast, UK.
- Naylor, D., Shannon, P., 2011. Petroleum geology of Ireland. Dunedin Academic Press Ltd., Edinburgh, UK.
- Pasquali, R., O'Neill, N., Reay, D., Waugh, T., 2010. The geothermal potential of Northern Ireland. In: Proceedings of the World Geothermal Congress 2010. 25–30 April 2010, Bali, Indonesia.
- Pellerin, L.D., Hohmann, G.W., 1990. Transient electromagnetic inversion; a remedy for magnetotelluric static shifts. *Geophysics* 55 (9), 1242–1250. <https://doi.org/10.1190/1.1442940>.
- Richardson, I., Neymeyer, A., 2013. Deep Geothermal Review Study: Final Report. Tech. rep. Department of Energy & Climate Change (DECC), London, United Kingdom.
- Scott, J.H., 1984. Computer Analysis of Digital Well Logs. Tech. Rep. 879. U.S. Geological Survey, Reston, VA, USA.
- Wilson, H.E., Manning, P.I., 1978. Geology of the Causeway Coast. British Geological Survey, Nottingham, UK.
- Young, M., 2016. Unearthed: Impacts of the Tellus Surveys of the North of Ireland. Royal Irish Academy.